Non-contrast power Doppler imaging with multidimensional clutter filtering for assessment of trans-arterial chemoembolization for hepatic malignancy

Ozgun, Kathryn, Tierney Stanton, Jaime, Baker, Jennifer, Borgmann, Anthony, Brown, Daniel, et al.

Kathryn Ozgun, Jaime Tierney Stanton, Jennifer Baker, Anthony Borgmann, Daniel Brown, Brett Byram, "Non-contrast power Doppler imaging with multidimensional clutter filtering for assessment of trans-arterial chemoembolization for hepatic malignancy," Proc. SPIE 11602, Medical Imaging 2021: Ultrasonic Imaging and Tomography, 116020N (15 February 2021); doi: 10.1117/12.2582109

SPIE.

Event: SPIE Medical Imaging, 2021, Online Only

Non-contrast power Doppler imaging with multidimensional clutter filtering for assessment of trans-arterial chemoembolization for hepatic malignancy

Kathryn Ozgun[a], Jaime Tierney Stanton[a], Jennifer Baker[b],
Anthony Borgmann[b], Daniel Brown[b], and Brett Byram[a]
[a]Department of Biomedical Engineering, Vanderbilt University
[b]Division of Interventional Radiology, Vanderbilt University Medical Center

ABSTRACT

Immediate postoperative assessment of trans-arterial chemoembolization (TACE) using gold standard modalities, MRI and CT, is unreliable due to confounding interactions with lipiodol and post-embolization inflammatory changes. We previously demonstrated that recent advancements in power Doppler ultrasound processing enables changes in slow blood flow to be detected immediately following TACE. Recently, we have developed a filtering method that employs a higher-order singular value decomposition (HOSVD) applied to aperture data to mitigate thermal noise and acoustic clutter. Here, we investigate HOSVD as a tool to improve non-contrast ultrasound evaluation of TACE. Preliminary feasibility is demonstrated in a small pilot study. Treatment-induced changes in perfusion are visualized most readily using the HOSVD filter in comparison to conventional filtering methods. The HOSVD filter produced the greatest change in contrast between pre-TACE and post-TACE power Doppler images.

Keywords: Blood flow, power Doppler, higher-order singular value decomposition (HOSVD), singular value decomposition (SVD), clutter rejection

1. INTRODUCTION

Over the last decade, liver cancer has become one of the primary causes of cancer-related death in the United States [1], [2]. Despite advances in clinical care, liver cancer remains associated with a high mortality because most cases are not eligible for curative surgical treatment, due to the advanced stage of disease at diagnosis. Global treatment guidelines endorse trans-arterial chemoembolization (TACE) as the standard therapy for palliative care and down-staging of hepatic malignancies [3]. The primary objective of TACE is to elicit occlusion of the tumor vascular supply while delivering high doses of chemotherapy. Therapeutic efficacy is determined by reduced contrast enhancement on MRI or CT, which correlates with tumor necrosis. However, therapeutic evaluation is not performed until 4-6 weeks posttreatment due to confounding interactions with the chemotherapeutic delivery agent, lipiodol, and post-embolization inflammatory changes [3], [4]. This delays response assessment and re-treatment of residual tumor which can result in tumor progression. A reliable, early assessment mechanism could improve survival.

Ultrasound imaging has been proposed for earlier assessment of TACE outcomes. Contrast-enhanced ultrasound (CEUS) can effectively detect perfusion changes indicative of therapeutic response 1-2 weeks post-TACE [5]–[7]. However, earlier assessment is susceptible to confounding interactions with gas deposits and drug-eluting beads. In addition, CEUS is dependent on contrast administration, which increases the complexity of intraprocedural imaging. In comparison, non-contrast power Doppler (PD) imaging is advantageous because the image is formed directly from the echo data and is more robust toward these confounding factors. Power Doppler was initially investigated for clinical evaluation of TACE nearly two decades ago, but motion artifacts and clutter signals from slowly moving tissue resulted in poor sensitivity toward blood flow [8]. Since then, advancements in imaging, filtering, and post-processing have enabled clinical visualization of low velocity blood flow.

Recent studies have demonstrated that non-contrast power Doppler imaging with these advanced techniques is sensitive to changes in perfusion immediately after TACE [9]–[12]. This suggests that non-contrast ultrasound may enable assessment of therapeutic efficacy 3-4 weeks earlier than conventional radiographic methods [13]. However, PD imaging remains susceptible to degradation caused by thermal noise and acoustic clutter signals. These sources of degradation

Medical Imaging 2021: Ultrasonic Imaging and Tomography, edited by Brett C. Byram,
Nicole V. Ruiter, Proc. of SPIE Vol. 11602, 116020N · © 2021 SPIE
CCC code: 1605-7422/21/$21 · doi: 10.1117/12.2582109

particularly impede robust microvasculature imaging, as low velocity blood echoes are often close to the noise floor and can exhibit similar temporal characteristics to clutter signals [14], [15].

To overcome these challenges, filtering is performed in ultrasonic blood flow imaging to suppress acoustic noise and "clutter" signals, which arise from reverberation, off-axis scattering, and tissue echoes [14], [16]. Conventionally, clutter rejection is achieved using IIR, FIR, and regression filters, which operate along temporal series of Doppler data [15], [17], [18]. More recently, singular value decomposition (SVD) has been used in clutter rejection algorithms [19]–[23]. Singular value decomposition is a method of adaptive basis generation, meaning that SVD filters are not constrained to the Fourier bases. Rather, the singular value decomposition produces two sets of singular vector matrices that characterize the temporal and spatial features of the data, which has enabled the development of numerous signal classification algorithms.

The higher-order singular value decomposition (HOSVD) has been proposed to further improve signal separation during filtering. The higher-order singular value decomposition is an extension of the singular value decomposition to data tensors [24]. Employing HOSVD in clutter rejection algorithms expands the feature space for signal classification, which enables better separability of the blood signal. The application of HOSVD for clutter rejection filtering was initially proposed by Kim et al., who developed an HOSVD filter that operated on a tensor of radiofrequency data with one spatial dimension and two slow-time dimensions [25]–[27]. Recently, we developed a HOSVD filtering technique for aperture domain data, which operates upon a tensor with a spatial dimension, slow-time dimension, and channel dimension [28]. In prior work, our aperture domain HOSVD filter was shown to enable greater rejection of clutter and noise signals in comparison to SVD filtering.

We propose the application of HOSVD filtering to improve visualization of treatment-induced changes in blood flow immediately following TACE. In addition, we seek to study if the changes in perfusion observed with PD are predictive of treatment outcome for TACE. In this proceedings, we demonstrate the efficacy of HOSVD filtering using data acquired in a small pilot study of eight subjects.

2. METHODS

2.1 Singular Value Decomposition Filtering

Singular value decomposition (SVD) is a matrix factorization technique that can be used to perform clutter rejection for blood flow imaging. Typically, SVD filters operate on radiofrequency data composed of Z axial samples, X lateral samples, and N slow-time frames. Prior to decomposition, the data is reshaped into a Casorati form ($M = XZ$), and can be represented as a 2-D matrix, $\boldsymbol{X} \in \mathbb{C}^{M \times N}$. The SVD of the 2-D radiofrequency data matrix is given by

$$\boldsymbol{X} = \boldsymbol{U}\,\boldsymbol{S}\,\boldsymbol{V}'$$

where (') indicates the transpose. SVD produces a singular value matrix, $\boldsymbol{S}$ and two unitary singular vector matrices $\boldsymbol{U}$ and $\boldsymbol{V}$. The singular vectors characterize the dominant features of the data along the spatial and temporal dimensions. The singular values indicate the scale of each singular vector. Filtering is performed by weighting or zeroing components that correspond to clutter signals.

2.2 Higher-Order Singular Value Decomposition Filtering

We have developed a HOSVD filter applied to a 3D tensor of aperture domain data, e.g. delayed channel data after synthetic transmit focusing, prior to the beam sum. The HOSVD filter operates on an aperture data tensor composed of Z axial samples, X lateral samples, N slow-time frames, and K channels. Combining the spatial samples in a Casorati form, the aperture data is represented as a 3-D matrix, $\boldsymbol{\mathcal{X}} \in \mathbb{C}^{M \times N \times K}$. The HOSVD of the 3-D aperture data matrix $\boldsymbol{\mathcal{X}} \in \mathbb{C}^{M \times N \times K}$ is given by

$$\boldsymbol{\mathcal{X}} = \boldsymbol{\mathcal{G}} \times_1 \boldsymbol{U} \times_2 \boldsymbol{V} \times_3 \boldsymbol{W}$$

where $\times_n$ indicates the mode-n product [24]. HOSVD yields a core tensor, $\boldsymbol{\mathcal{G}}$, and three unitary matrices: the spatial singular vectors, $\boldsymbol{U}$; the temporal singular vectors, $\boldsymbol{V}$; and the channel singular vectors, $\boldsymbol{W}$.

Clutter rejection was performed by reducing or zeroing components within the core tensor, $\mathcal{G}$, which map to clutter-dominant components. The composition of the core tensor and filter cutoffs were adaptively determined using a multidimensional classification scheme [28]. Signal classification was performed by analyzing (1) the mean frequency of temporal singular vectors, (2) the coherence characteristics of channel singular vectors, and (3) the energy of the spatial singular values.

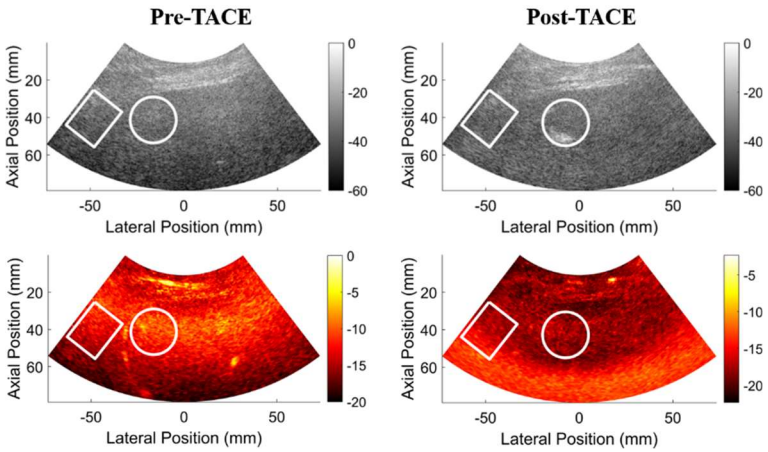

Figure 1. Example of ROIs for paired images. Regions exhibiting a comparable field of view and echogenicity in paired pre-TACE and post-TACE images were used for tumor (circle) and background (rectangle) regions of interest.

2.3 Clinical Data Acquisition

Eight patients undergoing TACE procedures were included in the IRB-approved study [11], [29]. The patient population involved six hepatocellular carcinoma cases and two neuroendocrine cases. Data were acquired at two timepoints, immediately before and immediately after the procedure. At each timepoint, three datasets were collected by the interventional radiologist performing the procedure. At clinical follow-up, the lesions were classified as progressive disease (PD), stable disease (SD), partial response (PR), or complete response (CR) using the modified Response Evaluation Criteria in Solid Tumors [13].

A Verasonics C5-2 probe with a 4.2 MHz center frequency was used to acquire 2 seconds (1200 frames) of channel data. The acquisition used a plane wave sequence composed of 9 angles evenly distributed over a span. The data were beamformed using plane wave synthetic focusing [30], yielding a net PRF of 600 Hz. For each dataset, an ensemble of 100 frames that maximized the average spatio-temporal correlation was selected in order to minimize the amount of out-of-frame motion. Adaptive demodulation was applied to reduce axial motion over the ensemble [31].

2.4 Data Processing

Processing and analysis were performed in Matlab (version R2018b, MathWorks, Natick, MA). Beamforming was implemented using the UltraSound ToolBox (v2.1) [32]. The TensorLab (v3.0) function *mlsvd* was used for HOSVD [33]. Power Doppler images were formed using the proposed HOSVD filter and a conventional SVD filter [11], [29]. For computational efficiency, processing was performed using sixteen randomly sampled blocks for both filters [34].

The SVD filter employed a lower and upper temporal cutoff as described by Song et al. [35]. The HOSVD filter employed four cutoffs: an equivalent lower and upper temporal cutoff, a channel cutoff, and a spatial cutoff. The upper temporal cutoffs and channel cutoff were determined adaptively [28]. The lower temporal cutoff was defined as the point where the mean singular vector frequency exceeds a specified cutoff frequency. For both filters, the lower temporal cutoff was parameterized using a cutoff frequency set between 15Hz and 40Hz in 5Hz increments. The same cutoff frequency was used for paired pre-TACE and post-TACE datasets. The spatial cutoff was defined as the point where the singular value energy begun to plateau. This point indicated the transition to dominantly noise-bearing singular values, which follow a Marchenko–Pastur distribution [36]. The spatial cutoff was parameterized by a normalized decay rate of either 0.015 or 0.025, manually chosen so that small vessel structure was preserved.

Since power measurements may vary between clinical scans due to field-of-view and attenuative effects, an assessment of treatment-derived changes in blood flow was performed using semi-quantitative metrics. Image quality was measured for each image using the tumor-to-background contrast, as shown in (1)(1). Since the background region power is approximately stable at both timepoints, the normalization by background power in the contrast measurement compensates for attenuative and transducer effects [37]. Tumor and background ROIs that depicted a comparable echogenicity and view were selected to facilitate a fair comparison between paired pre-TACE and post-TACE images, as shown in Figure 1. The

relative change in contrast was measured as $Contrast_{pre} - Contrast_{post}$, which was expected to produce a positive net difference if flow was suppressed in the tumor region during TACE.

$$Contrast = 10 * \log_{10}\left(\frac{\frac{1}{M}\sum_{i=1}^{M} PD_{tumor}(i)}{\frac{1}{N}\sum_{i=1}^{N} PD_{background}(i)}\right) \quad (1)$$

RESULTS

After the TACE procedure, a decrease in tumor-to-background contrast and tumor-region power was observed for both filters, as shown in Figure 2. Since the TACE procedure is performed to achieve vascular stasis within the tumor, we anticipate that this change is indicative of flow suppression. This aligns with clinical follow-up assessment, which indicated the cohort was composed of 2 partial response cases and 6 complete response cases at the first follow-up timepoint.

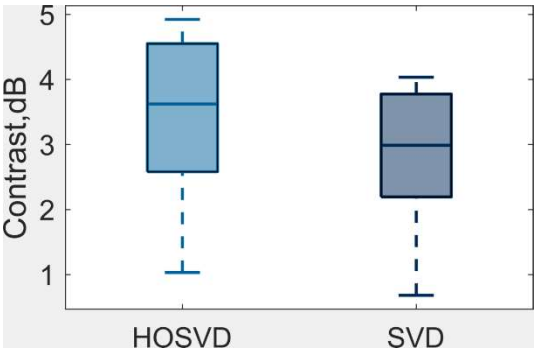

Figure 2: Image Quality Results. The HOSVD filter yielded a greater change in tumor-to-background contrast between pre-TACE and post-TACE images than the SVD filter, which is consistent with the greater background suppression incurred by HOSVD filtering.

Examples of the pilot study cases are shown in Figure 3. Due to lipiodol deposition, the post-TACE B-mode images present with hyperechoic structure in the tumor region. Clutter rejection filtering effectively removes the stationary hyperechoic signal, which enables visualization of residual blood flow immediately after TACE. HOSVD produced a greater average change in contrast after treatment (3.43 $\pm$ 1.36 dB) in comparison to SVD (2.83 $\pm$ 1.17 dB). Qualitatively, the HOSVD-filtered case produced improved discrimination of tumor borders and achieved greater suppression of thermal noise.

The lesions depicted in Figure 4 presented with reduced vascularity and were classified as partial response at first follow-up using contrast-enhanced imaging. However, tumor burden subsequently increased, and the lesions were classified as progressive disease at a subsequent follow up. The post-TACE PD images shown in Figure 4. exhibit with residual vascularity close to the tumor site, indicated by the yellow arrows, which may be an indication of remaining feeder vasculature. In the future, an assessment of a larger HCC patient cohort will be performed to assess the relationship between disease progression and post-TACE PD enhancement.

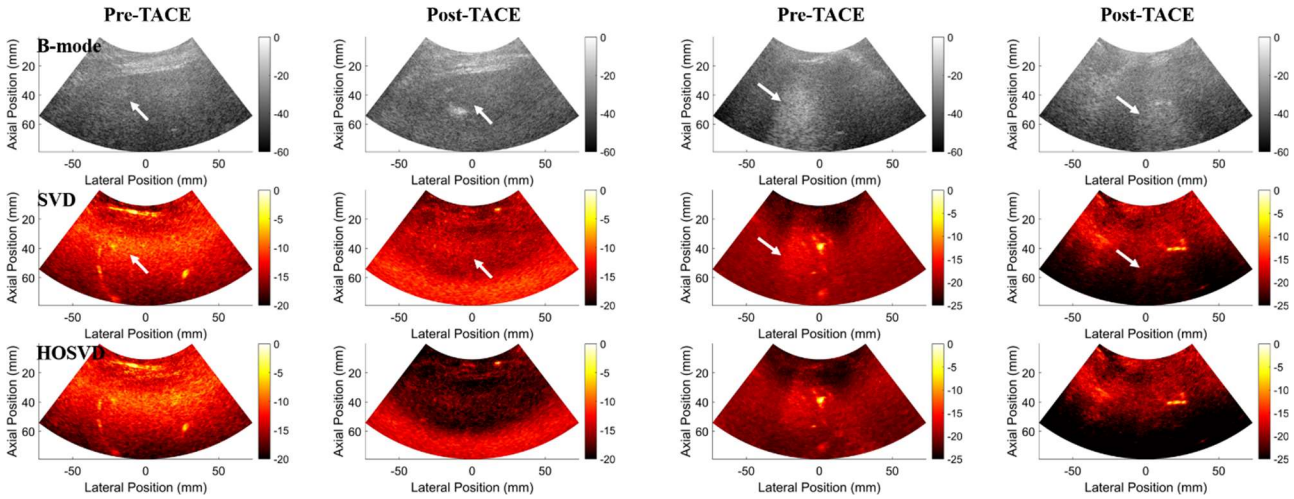

Figure 3. **Sample TACE images with SVD and HOSVD filtering**. Two clinical cases are shown to demonstrate paired pre-TACE and post-TACE images. Power Doppler images formed using the HOSVD filter (bottom row) exhibit less clutter than the power Doppler images formed using the SVD filter (middle row). The white arrows indicate tumor location.

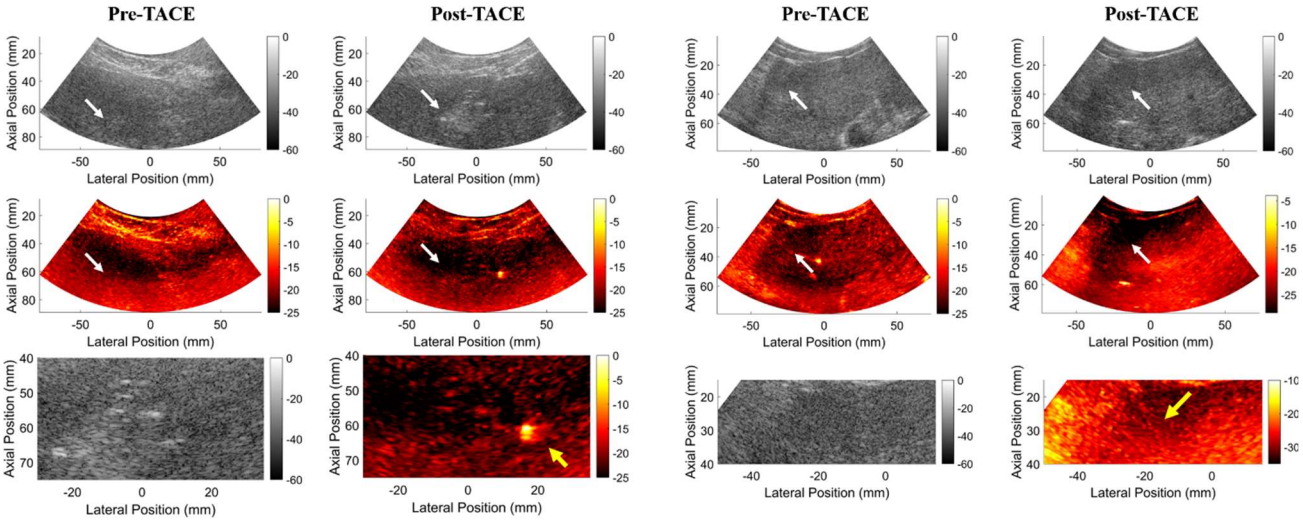

Figure 4. Paired TACE images with residual vascularity. Two of the lesions were classified as partial response at the first follow-up, with disease progression at later follow-up timepoints. In the post-TACE power Doppler images formed using HOSVD filtering, residual vascularity can be observed near the tumor region (yellow arrows).

3. CONCLUSIONS

This pilot study demonstrates that coupling PD imaging with advanced clutter filtering can be used to observe changes in low velocity blood flow after TACE. The proposed HOSVD filtering technique yielded greater suppression of clutter and noise in comparison to SVD filtering. Further, the HOSVD filter produced greater measured changes in contrast and tumor-region power between pre-TACE and post-TACE images, which suggests that HOSVD may improve assessment of procedural endpoints.

These findings are supported by prior work, in which HOSVD produced improvement over conventional SVD filtering for imaging of arteriole level flow (~10mm/sec [38]), observed in simulation and *in vivo* [28]. TACE additionally occludes perfusion level and low velocity blood flow which has been observed using ultrasound in preliminary studies [9], [11], [39]. Low velocity blood flow may be observed as a blush rather than structured vasculature [40], so future studies are needed to assess if HOSVD effectively retains perfusion-level flow. To further characterize sensitivity of PD imaging toward low velocity blood flow, we plan to develop branching vessel simulations that mimic the environment of the tumor.

Overall, non-contrast power Doppler ultrasound is a potential solution for immediate evaluation of vascular stasis achieved during TACE procedures. In combination with advanced beamforming and filtering techniques, PD imaging is sensitive to changes in low velocity flow that occur during TACE. We demonstrate preliminary feasibility of HOSVD filtering using clinical data obtained in a small pilot study. In power Doppler images formed using HOSVD filtering, the observed presence of residual vascularity may be indicative of longitudinal disease progression. In future work, we intend to have observers or radiologists blinded to follow-up outcome assess extent of residual vascularity based on enhancement in post-TACE PD images. These preliminary findings suggest that the application of HOSVD filtering may improve slow flow visualization and could enable non-contrast ultrasound evaluation for TACE.

4. ACKNOWLEDGEMENTS

This work was supported in part by the National Institute of Biomedical Imaging and Bioengineering under Grant T32-EB021937, and in part by the National Science Foundation Award under Grant IIS-1750994. The authors would like to thank the staff of the Vanderbilt University ACCRE computing resource and the contributors to the UltraSound ToolBox.

REFERENCES

[1] "Annual report to the nation on the status of cancer, part I: National cancer statistics - Henley - 2020 - Cancer - Wiley Online Library." Accessed: Jan. 22, 2021. [Online]. Available: https://acsjournals.onlinelibrary.wiley.com/doi/10.1002/cncr.32802.

[2] R. L. Siegel, K. D. Miller, and A. Jemal, "Cancer statistics, 2019," *CA. Cancer J. Clin.*, vol. 69, no. 1, pp. 7–34, 2019, doi: https://doi.org/10.3322/caac.21551.

[3] "Gaba et al. - 2017 - Quality Improvement Guidelines for Transarterial C.pdf." Accessed: Jan. 22, 2021. [Online]. Available: https://servei.org/wp-content/uploads/2017-JVIR-TACE-Guidelines.pdf.

[4] R. Lencioni and J. M. Llovet, "Modified RECIST (mRECIST) assessment for hepatocellular carcinoma," *Semin. Liver Dis.*, vol. 30, no. 1, pp. 52–60, Feb. 2010, doi: 10.1055/s-0030-1247132.

[5] K. Nam *et al.*, "Evaluation of hepatocellular carcinoma transarterial chemoembolization using quantitative analysis of 2D and 3D real-time contrast enhanced ultrasound," *Biomed. Phys. Eng. Express*, vol. 4, no. 3, p. 035039, Apr. 2018, doi: 10.1088/2057-1976/aabb14.

[6] Z. Sparchez, T. Mocan, P. Radu, O. Anton, and N. Bolog, "Contrast enhanced ultrasonography in assessing the treatment response to transarterial chemoembolization in patients with hepatocellular carcinoma," *Med. Ultrason.*, vol. 18, no. 1, pp. 96–102, Mar. 2016, doi: 10.11152/mu.2013.2066.181.scz.

[7] H. Moschouris, K. Malagari, I. Kornezos, M. G. Papadaki, P. Gkoutzios, and D. Matsaidonis, "Unenhanced and Contrast-Enhanced Ultrasonography During Hepatic Transarterial Embolization and Chemoembolization With Drug-Eluting Beads," *Cardiovasc. Intervent. Radiol.*, vol. 33, no. 6, pp. 1215–1222, Dec. 2010, doi: 10.1007/s00270-010-9918-7.

[8] K. Kubota *et al.*, "Evaluation of hepatocellular carcinoma after treatment with transcatheter arterial chemoembolization: comparison of Lipiodol-CT, power Doppler sonography, and dynamic MRI," *Abdom. Imaging*, vol. 26, no. 2, pp. 184–190, Mar. 2001, doi: 10.1007/s002610000139.

[9] J. Tierney, J. Baker, A. Borgmann, D. Brown, and B. Byram, "Non-contrast power Doppler ultrasound imaging for early assessment of trans-arterial chemoembolization of liver tumors," *Sci. Rep.*, vol. 9, no. 1, p. 13020, Dec. 2019, doi: 10.1038/s41598-019-49448-8.

[10] J. Tierney, K. Walsh, H. Griffith, J. Baker, D. B. Brown, and B. Byram, "Combining Slow Flow Techniques With Adaptive Demodulation for Improved Perfusion Ultrasound Imaging Without Contrast," *IEEE Trans. Ultrason. Ferroelectr. Freq. Control*, vol. 66, no. 5, pp. 834–848, May 2019, doi: 10.1109/TUFFC.2019.2898127.

[11] J. Tierney, J. Baker, K. Ozgun, A. Borgmann, D. Brown, and B. Byram, "Non-Contrast Perfusion Ultrasound Imaging for Assessment of Trans-Arterial Chemoembolization for Hepatic Malignancy," in *2018 IEEE International Ultrasonics Symposium (IUS)*, Kobe, Oct. 2018, pp. 1–3, doi: 10.1109/ULTSYM.2018.8579939.

[12] J. Tierney, J. Baker, D. Brown, D. Wilkes, and B. Byram, "Independent Component-Based Spatiotemporal Clutter Filtering for Slow Flow Ultrasound," *IEEE Trans. Med. Imaging*, pp. 1–1, 2019, doi: 10.1109/TMI.2019.2951465.

[13] A. Arora and A. Kumar, "Treatment Response Evaluation and Follow-up in Hepatocellular Carcinoma," *J. Clin. Exp. Hepatol.*, vol. 4, pp. S126–S129, Aug. 2014, doi: 10.1016/j.jceh.2014.05.005.

[14] A. Heimdal and H. Torp, "Ultrasound doppler measurements of low velocity blood flow: limitations due to clutter signals from vibrating muscles," *IEEE Trans. Ultrason. Ferroelectr. Freq. Control*, vol. 44, no. 4, pp. 873–881, Jul. 1997, doi: 10.1109/58.655202.

[15] S. Bjaerum, H. Torp, and K. Kristoffersen, "Clutter filters adapted to tissue motion in ultrasound color flow imaging," *IEEE Trans. Ultrason. Ferroelectr. Freq. Control*, vol. 49, no. 6, pp. 693–704, Jun. 2002, doi: 10.1109/TUFFC.2002.1009328.

[16] F. W. Mauldin, D. Lin, and J. A. Hossack, "The Singular Value Filter: A General Filter Design Strategy for PCA-Based Signal Separation in Medical Ultrasound Imaging," *IEEE Trans. Med. Imaging*, vol. 30, no. 11, pp. 1951–1964, Nov. 2011, doi: 10.1109/TMI.2011.2160075.

[17] H. Torp, "Clutter rejection filters in color flow imaging: a theoretical approach," *IEEE Trans. Ultrason. Ferroelectr. Freq. Control*, vol. 44, no. 2, pp. 417–424, Mar. 1997, doi: 10.1109/58.585126.

[18] S. Bjaerum, H. Torp, and K. Kristoffersen, "Clutter filter design for ultrasound color flow imaging," *IEEE Trans. Ultrason. Ferroelectr. Freq. Control*, vol. 49, no. 2, pp. 204–216, 2002.

[19] U.-W. Lok *et al.*, "Real time SVD-based clutter filtering using randomized singular value decomposition and spatial downsampling for micro-vessel imaging on a Verasonics ultrasound system," *Ultrasonics*, vol. 107, p. 106163, Sep. 2020, doi: 10.1016/j.ultras.2020.106163.

[20] G. G. Olleros, C. A. Villagómez Hoyos, K. L. Hansen, M. B. Stuart, and J. A. Jensen, "Spatiotemporal Filtering for Synthetic Aperture Slow Flow Imaging," in *2018 IEEE International Ultrasonics Symposium (IUS)*, Oct. 2018, pp. 1–4, doi: 10.1109/ULTSYM.2018.8579611.
[21] J. Baranger, B. Arnal, F. Perren, O. Baud, M. Tanter, and C. Demene, "Adaptive Spatiotemporal SVD Clutter Filtering for Ultrafast Doppler Imaging Using Similarity of Spatial Singular Vectors," *IEEE Trans. Med. Imaging*, vol. 37, no. 7, pp. 1574–1586, Jul. 2018, doi: 10.1109/TMI.2018.2789499.
[22] A. Yu and L. Lovstakken, "Eigen-based clutter filter design for ultrasound color flow imaging: a review," *IEEE Trans. Ultrason. Ferroelectr. Freq. Control*, vol. 57, no. 5, pp. 1096–1111, May 2010, doi: 10.1109/TUFFC.2010.1521.
[23] A. J. Y. Chee and A. C. H. Yu, "Receiver-Operating Characteristic Analysis of Eigen-Based Clutter Filters for Ultrasound Color Flow Imaging," *IEEE Trans. Ultrason. Ferroelectr. Freq. Control*, vol. 65, no. 3, pp. 390–399, Mar. 2018, doi: 10.1109/TUFFC.2017.2784183.
[24] L. De Lathauwer, B. De Moor, and J. Vandewalle, "A Multilinear Singular Value Decomposition," *SIAM J. Matrix Anal. Appl.*, vol. 21, no. 4, pp. 1253–1278, Jan. 2000, doi: 10.1137/S0895479896305696.
[25] M. Bayat, A. Alizad, and M. Fatemi, "Multi-rate higher order singular value decomposition for enhanced non-contrast ultrasound Doppler imaging of slow flow," in *2018 IEEE 15th International Symposium on Biomedical Imaging (ISBI 2018)*, Apr. 2018, pp. 1178–1181, doi: 10.1109/ISBI.2018.8363781.
[26] M. Kim, Y. Zhu, J. Hedhli, L. W. Dobrucki, and M. F. Insana, "Multidimensional Clutter Filter Optimization for Ultrasonic Perfusion Imaging," *IEEE Trans. Ultrason. Ferroelectr. Freq. Control*, vol. 65, no. 11, pp. 2020–2029, Nov. 2018, doi: 10.1109/TUFFC.2018.2868441.
[27] M. Kim, C. K. Abbey, J. Hedhli, L. W. Dobrucki, and M. F. Insana, "Expanding Acquisition and Clutter Filter Dimensions for Improved Perfusion Sensitivity," *IEEE Trans. Ultrason. Ferroelectr. Freq. Control*, vol. 64, no. 10, pp. 1429–1438, Oct. 2017, doi: 10.1109/TUFFC.2017.2719942.
[28] K. Ozgun and B. Byram, "A Channel Domain Higher-Order SVD Clutter Rejection Filter for Small Vessel Ultrasound Imaging," in *2020 IEEE International Ultrasonics Symposium (IUS)*, Sep. 2020, pp. 1–4, doi: 10.1109/IUS46767.2020.9251419.
[29] J. Tierney, J. Baker, A. Borgmann, D. Brown, and B. Byram, "Non-contrast power Doppler ultrasound imaging for early assessment of trans-arterial chemoembolization of liver tumors," *Sci. Rep.*, vol. 9, no. 1, Art. no. 1, Sep. 2019, doi: 10.1038/s41598-019-49448-8.
[30] G. Montaldo, M. Tanter, J. Bercoff, N. Benech, and M. Fink, "Coherent plane-wave compounding for very high frame rate ultrasonography and transient elastography," *IEEE Trans. Ultrason. Ferroelectr. Freq. Control*, vol. 56, no. 3, pp. 489–506, Mar. 2009, doi: 10.1109/TUFFC.2009.1067.
[31] J. Tierney, C. Coolbaugh, T. Towse, and B. Byram, "Adaptive Clutter Demodulation for Non-Contrast Ultrasound Perfusion Imaging," *IEEE Trans. Med. Imaging*, vol. 36, no. 9, pp. 1979–1991, Sep. 2017, doi: 10.1109/TMI.2017.2714901.
[32] A. Rodriguez-Molares *et al.*, "The UltraSound ToolBox," in *2017 IEEE International Ultrasonics Symposium (IUS)*, Washington, DC, Sep. 2017, pp. 1–4, doi: 10.1109/ULTSYM.2017.8092389.
[33] Vervliet N., Debals O., Sorber L., Van Barel M. and De Lathauwer L., "Tensorlab | A Matlab package for tensor computations." https://www.tensorlab.net/ (accessed Apr. 23, 2020).
[34] P. Song *et al.*, "Accelerated Singular Value-Based Ultrasound Blood Flow Clutter Filtering With Randomized Singular Value Decomposition and Randomized Spatial Downsampling," *IEEE Trans. Ultrason. Ferroelectr. Freq. Control*, vol. 64, no. 4, pp. 706–716, Apr. 2017, doi: 10.1109/TUFFC.2017.2665342.
[35] P. Song, A. Manduca, J. D. Trzasko, and S. Chen, "Ultrasound Small Vessel Imaging With Block-Wise Adaptive Local Clutter Filtering," *IEEE Trans. Med. Imaging*, vol. 36, no. 1, pp. 251–262, Jan. 2017, doi: 10.1109/TMI.2016.2605819.
[36] R. R. Nadakuditi and A. Edelman, "Sample Eigenvalue Based Detection of High-Dimensional Signals in White Noise Using Relatively Few Samples," *IEEE Trans. Signal Process.*, vol. 56, no. 7, pp. 2625–2638, Jul. 2008, doi: 10.1109/TSP.2008.917356.
[37] J. M. Rubin, R. O. Bude, J. B. Fowlkes, R. S. Spratt, P. L. Carson, and R. S. Adler, "Normalizing fractional moving blood volume estimates with power Doppler US: defining a stable intravascular point with the cumulative power distribution function.," *Radiology*, vol. 205, no. 3, pp. 757–765, Dec. 1997, doi: 10.1148/radiology.205.3.9393532.
[38] J. A. Jensen, *Estimation of blood velocities using ultrasound: a signal processing approach*. Cambridge ; New York, USA: Cambridge University Press, 1996.

[39] J. Tierney, K. Walsh, H. Griffith, J. Baker, D. B. Brown, and B. Byram, “Combining Slow Flow Techniques With Adaptive Demodulation for Improved Perfusion Ultrasound Imaging Without Contrast,” *IEEE Trans. Ultrason. Ferroelectr. Freq. Control*, vol. 66, no. 5, pp. 834–848, May 2019, doi: 10.1109/TUFFC.2019.2898127.
[40] R. O. Bude, J. M. Rubin, and R. S. Adler, “Power versus conventional color Doppler sonography: comparison in the depiction of normal intrarenal vasculature.,” *Radiology*, vol. 192, no. 3, pp. 777–780, Sep. 1994, doi: 10.1148/radiology.192.3.8058946.